Binding of a positive allosteric modulator CDPPB to metabotropic glutamate receptor type 5 (mGluR5) probed by all-atom molecular dynamics simulations

Abdullahi Ibrahim Uba¹, John Chea², Hannah Hoag¹, Mariya Hryb¹, Candice Bui-Linh¹, and Chun Wu¹*

¹College of Science and Mathematics, Rowan University, Glassboro, NJ, 08028, United States.

²College of Engineering, Rowan University, Glassboro, NJ, 08028, United States.

*To whom correspondence should be addressed: wuc@rowan.edu

Abstract

Positive allosteric modulators (PAMs) of metabotropic glutamate receptor type 5 (mGluR5) potentiate positive receptor response and may be effective for the treatment of schizophrenia and cognitive disorders. Although crystal structures of mGluR5 complexed with the negative allosteric modulators (NAMs) are available, no crystal structure of mGluR5 complexed with PAM has been reported to date. Thus, conformational changes associated with the binding of PAMs to mGluR5 remain elusive. Here, a PAM CDPPB, and two NAMs MTEP and MFZ10-7 used as a negative control, were docked to the crystal structure. The docked complexes were submitted to molecular dynamics simulations to examine the activation of the PAM system. An MM/GBSA binding energy calculation was performed to estimate binding strength. Furthermore, molecular switch analysis was done to get insights into conformational changes of the receptor. The PAM CDPPB displays a stronger binding affinity for mGluR5 and induces conformational changes. Also, a salt bridge between TM3 and TM7, corresponding to the ionic lock switch in class A GPCRs is found to be broken. The PAM-induced receptor conformation is more like the agonist-induced conformation than the antagonist-induced conformation, suggesting that PAM works by inducing conformation change and stabilizing the active receptor conformation. **Keywords**: metabotropic glutamate receptor type 5 (mGluR5), Positive allosteric modulators (PAMs), negative allosteric modulators (NAMs), PAM CDPPB, MD simulation

Introduction

Metabotropic glutamate receptor type 5 (mGluR5) is a member of class C G protein-coupled receptors that plays a modulatory role in the central nervous system [1-4]. mGluR5 is a known signaling partner with N-methyl-D-aspartate (NMDA) receptors allowing them to co-regulate one another [5]. mGluR5 is implicated in psychological disorders, such as addiction [6] and anxiety [7].

mGluR5 is a 1212 amino acid long protein (**Figure S1**) folded into 3 structural domains: N-terminal extracellular domain (ECD) referred to as the "venus trap domain" where ligands bind to activate or inactivate the receptor, a 7-transmembrane domain (TMD) where allosteric modulators bind to, and the C-terminal intracellular domain that makes contact with G-protein (Figures S2-3) [8]. Binding to the allosteric site on TMD can allow a modulator ligand to potentiate receptor activity via a positive allosteric modulator (PAM) or inhibit receptor activity via a negative allosteric modulator (NAM) [9, 10]. So far, NAM dipraglurant has been approved by U. S. FDA as an orphan drug for the treatment of Levodopa-induced Dyskinesia (PD-LID) in 2016 [11] and more NAMs are undergoing clinical trials. For example, a NAM mavoglurant is in phase III clinical trial and has demonstrated promising effects on fragile X syndrome [12]. In the continuous search for mGlu5R modulators with improved potency, more lead compounds are being used for research purposes. For instance, MTEP (3-((2-Methyl-4-thiazolyl)ethynyl) pyridine) as a NAM of mGluR5, is considered a leading compound for new drugs that are specifically effective on mGluR5.[13] MFZ10-7 (3-Fluoro-5-[2-(6-methyl-2pyridinyl)ethylnyl]benzonitrile hydrochloride) is another high-affinity NAM targeting mGluR5. It is known to bind to the mGluR5 with higher potency than MTEP [14]. On the other hand, positive allosteric modulation of metabotropic mGluR5 is equally promising for the treatment of

schizophrenia and cognitive disorders [15]. PAMs can reverse cognitive deficits and behavioral and electrophysiological changes produced by NMDA receptor antagonists, thereby showing potential for treating schizophrenia and drug addiction [16, 17]. CDPPB (3-cyano-N-(1,3-diphenyl-1H-pyrazole-5-yl)benzamide) is a PAM that potentiates mGluR5 responses by binding to the allosteric site of mGluR5 and is known to compete with NAM MPEP [18], with high potency (EC₅₀ values of 25-100 nM) [19].

The available complex structures of the mGluR5 with agonists, antagonists (Table S1), and NAMs—including mavoglurant (PDB ID: 4009) (Figure 1) [20-23], provide insights into different responses of the receptor due to the binding different ligands/modulators. Without an allosteric modulator, the agonist and antagonist crystal structures show large conformational differences at both the ECD and TMD (5.2 Å), suggesting that TMD is a key responsible domain, and its active conformation is very different to its inactive conformation. The crystal structure of mGluR5 TMD bound by a NAM mavoglurant (PDB ID: 4009) differs from the TMD of the apo form (PDB ID: 6N52), agonist (PDB ID: 6N51), and antagonist (PDB ID: 3FD9) bound mGluR5 by RMSD values 3.09 Å, 3.59 Å, and 4.2 Å, respectively, suggesting that NAM appears to stabilize the inactive conformation. At present, there are no crystal structures of mGluR5 in complex with PAM, hence the binding effects of the PAM is not fully understood.

To address this question, we built the complexes of mGluR5 with a PAM ligand (CDPPB) and two NAM ligands (MTEP and MFZ10-7) using molecular docking (Figure 1) and examined the binding-induced conformational changes of the receptor using molecular dynamics (MD) simulations. Furthermore, we estimated their binding affinity using MM/GBSA binding energy calculation method. This study is aimed at elucidating the binding of PAM CDPPB, which may ultimately aid in the design of better PAM as drug candidates for cognitive disorders.

Methods

System setup and docking

The ligand structures of NAMs MTEP and MFZ10-7, and PAM CDPPB were downloaded from the ZINC database. The two NAM ligands were used to increase the chance of predicting specific PAM CDPPB-induced conformational changes. On the other hand, only a PAM ligand was used because CDPPB is known to compete with one of the most potent NAM ligands, the MPEP. Thus, CDPPB can be a good representative PAM ligand [18]. The ligands were prepared using Maestro (Schrödinger Inc.), in which Epik (empirical pKa prediction) calculation was done to pick the most abundantly charged state. Ligand geometric minimization was done to minimize the potential energy.

The crystal structure of mGluR5 complexed with negative allosteric modulator mavoglurant (PDB ID: 4009) was retrieved from the Protein Data Bank (www.rcsb.org/pdb) [24] and prepared using the protein preparation wizard in Maestro [25]. During the preparation, missing hydrogen atoms and missing side chain atoms were added, correct bond orders were assigned, disulfide bonds were created, and water molecules beyond 5 Å were deleted. The charge state of the titratable residues was optimized using PROPKA at pH of 7. Finally, a restrained minimization was done to relax the protein using an OPLS3 force field [26]. A docking grid was generated using the coordinates of the cocrystal ligand mavoglurant in the crystal structure, 4009. Docking was performed using Glide extra precision (XP) docking scoring function in the Maestro program [27].

Molecular dynamics simulation setup

The complexes were aligned to the membrane set to the helices of the TMD using the OPM server [28]. Each complex was placed in a biologically relevant membrane of

phosphatidylcholine (POPC) lipids [29] and solvated in the SPC water model, neutralized by the addition of Na⁺ ions and at a concentration of 0.15 M NaCl, and modeled using the OPLS3 force field [26] in the Desmond simulation package.

Molecular dynamics simulation

Like successfully applied to another GPCR structures previously [30, 31], the default Desmond relaxation protocol [32] consisting of multiple stages was applied to relax the system. Three independent 1000 ns-production runs were carried out for each system under the NPT ensemble. The temperature was controlled using the Nosé-Hoover chain coupling scheme [33] with a coupling constant of 1.0. The pressure was controlled using the Martyna-Tuckerman-Klein chain coupling scheme [33] with a coupling constant of 2.0 ps. M-SHAKE [34] was applied to constrain all bonds connecting hydrogen atoms. The long-range electrostatic interactions were treated using the k-space Gaussian split Ewald method [35]. Long-range van der Waals interactions were based on a uniform density approximation. The cutoff of the short-range non-bonded interaction was set to 10 Å. An r-RESPA integrator [36] was used to calculate non-bonded forces. Short-range forces were updated every step and the long-range forces every 3 steps. A time step of 2.0 fs time was used, and snapshots were collected every 50.0 ps.

Molecular dynamics simulation results analysis

To check the convergence of the MD simulations, Cα protein and ligand RMSDs, RMSFs, protein secondary structure elements, and protein-ligand contacts were computed using the whole trajectories. To determine the dominant structure, the 3 trajectories for each system were combined, and trajectory clustering analysis was performed using the Desmond trajectory clustering tool [37]. Hierarchical clustering method with average linkage, using backbone RMSD

as the structural similarity with merging distance cutoff set at 2.5 Å, was applied. The centroid of each cluster—the structure with the greatest number of neighbors in the structural family, is considered the representative structure of each cluster.

MM/GBSA binding energy calculations and decomposition

Molecular mechanics generalized Born surface area (MM/GBSA) binding energy calculation is considered as an efficient and reliable free energy simulation method to model protein-ligand interaction [38]. Therefore, MM/GBSA energy was calculated on the snapshots obtained during the last 20 ns for each complex using the surface-area-based generalized Born model with an implicit membrane (VSGB 2.0) [39, 40].

The default procedure consists of three steps: computation of energies of receptor alone, ligand alone, and receptor-ligand complex. The interaction terms are Coulombic, H-bond, GB solvation, van der Waals, pi-pi packing, self-contact, and lipophilic interactions. The total binding free energy equation is given as:

$$\Delta E_{\text{(bind)}} = E_{\text{complex}} - (E_{\text{ligand}} + E_{\text{receptor}})$$

The interaction terms were then merged into three components, Electrostatics, E_{vdW} , and $E_{lipophilic}$, where

$$E_{electrostatics} = H_{bond} + E_{coulomb} + E_{GB solvation}$$

$$E_{vdW} = E_{vdW} + E_{\pi\text{-}\pi} + E_{self\text{-contact}} \ and \ E_{lipophilic}$$

Results

The PAM CDPPB displays stronger binding to mGluR5

The allosteric site of mGluR5 is ~ 8 Å from the receptor's surface and is composed mainly of hydrophobic pocket defined by Ile651^{3.36}, Pro655^{3.40}, Leu744^{5.44}, and Asn747^{5.47},

Trp785^{6.50}, Phe788^{6.53}, Met802^{7.32}, Val806^{7.36}. Analysis of docking poses reveals that the PAM CDPPB binds less deep and occupies a greater space in the pocket. On the other hand, the docking site and poses of the NAMs are very similar to that of the cocrystal ligand, NAM mavoglurant (**Figure 1**). Figures S4 and S5 show the contribution of the individual residues for each system. Consistent with experimental data [19], the PAM CDPPB displays stronger binding than both NAMs. The binding energy scores are estimated to be -10.3, -9.5, and -6.9 kcal/mol for the PAM CDPPB, NAMs MFZ10-7 and MTEP, respectively (**Table 1**).

MD Simulations and MM/GBSA Binding Energy

The stability of each docked complex was examined through 3 x1000 ns MD simulation and RMSD was used as a measure of structural stability. Both protein-Cα and ligand RMSDs converge through the simulation (**Figure 2**). The RMSDs from the three individual trajectories of each system are included in the supporting document (**Figures S6-S8**). Consistent with the docking scores, the estimated MM/GBSA binding energy of CDPPB is higher than those of the two NAMs (**Table 1**). Considering MTEP as the reference ligand, ΔVDW of MFZ10-7's is found to be -5.4 kcal/mol stronger, while that of CDPPB is -22.7 kcal/mol stronger. A similar trend is seen with ΔGBELE. The residual contribution to the docking MM/GBSA binding energy score is tabulated (**Table 2**). Residues with negligible protein-ligand MM/GBSA scores were excluded from this list.

Inspection of ligand pose after MD simulations shows a slightly more conformational adjustment for the NAMs compared to the PAM CDPPB (Figure 3). Also, the PAM CDPPB-bound mGluR5 appears to open outward at the intracellular domain. On the other hand, the MFZ10-7 bound structure appears to maintain its original conformation, suggesting greater stability.

Table 1. MM/GBSA binding energies (kcal/mol) for NAMs MTEP, MFZ10-7, and PAM CDPPB against mGluR5.

Ligand	VDW	ΔVDW	GBELE	ΔGBELE	LIPO	ΔLΙΡΟ	ΔG	$\Delta\Delta G$	XP	ΔG	IC50	ΔG	$\Delta\Delta G$
							(MM/GBSA)	(MM/GBSA)	Score	(XP	(nM)	(Experime	(Experime
										Score)		ntal)	ntal)
MTEP	-40.9±1.6	0.0	-6.9±2.2	0.0	-35.5±1.2	0.0	-83.3±2.9	0.0	-6.9	0.0	110	-9.6	0.0
MFZ10-7	-46.3±1.8	-5.40	-8.2±3.7	-1.3	-33.0±0.7	2.5	-87.5±4.1	-4.2	-9.5	-2.6	2.4	-11.8	-2.3
CDPPB	-63.6±2.0	-22.7	-16.8±2.8	-9.9	-44.6±1.4	-9.1	-125±3.7	-41.7	-10.3	-3.4			

¹ VDW: change of van der Waals energy in gas phase upon complex formation

² **AVDW:** relative van der Waals energy with reference, MTEP system.

³ **GBELE:** change of electrostatic interactions (GB/Generalized Born electrostatic solvation energy+ ELE/Coulomb energy +Hydrogen-bonding) upon complex formation.

⁴ **ΔGBELE:** relative electrostatic energy with reference to an active complex. MTEP system is set as a reference.

⁵ **LIPO:** change of lipophilic term (Lipophilic energy) upon complex formation.

⁶ **ΔLIPO:** relative hydrophobic energy with reference to MTEP system.

⁷ ΔG (MM/GBSA): MM/GBSA binding energy (Complex – Receptor – Ligand). This result does not factor in the entropy term so $\Delta G = \Delta H$

⁸ ΔΔG (MM/GBSA): relative binding energy with MTEP's binding energy.

⁹ **XP Score:** strength of non-covalent interaction (binding affinity) between ligand and protein after docking.

 $^{^{10}}$ Δ G (XP Score): docking score comparison with MTEP system.

¹¹ **IC50**: experimental IC50 values.

¹² **ΔG (Experimental):** free binding energy that factors in entropy term. $\Delta G = -RT \ln K$, where R = 0.00198588 mol*K, T = 300K, K is the reported IC50 value in mol.

¹³ ΔΔG (Experimental): relative free binding energy with MTEP system.

Table 2. XP Docking score and MM/GBSA score are listed to show the contribution of each residue in the docking process. Residues shown in bold are crucial residues with persistent interactions through the simulations.

	MTEP	XP	MM/GB	MFZ10-	XP	MM/GB	CDPPB	XP	MM/GBS
		SCORE	SA	7	SCORE	SA		SCORE	Α
			SCORE			SCORE			SCORE
GEN-					7TM				
NO									
2.49	GLY624	-0.9	-0.7	GLY624	-1.4	-0.8	GLY624	-2.0	-0.6
2.50	ILE625	-1.8	-2.3	ILE625	-1.8	-1.5	ILE625	-2.6	-1.1
2.53	GLY628	-0.9	-0.7	GLY628	-0.1	-0.4	GLY628	-0.2	-0.2
3.29	ARG648	0.3	0.2	ARG648	-0.7	-0.4	ARG648	0.2	0.3
3.31	GLY650	-0.1	-0.1	GLY650	-0.3	-0.2	GLY650	-0.5	-0.5
3.32	ILE651	-0.7	-1.2	ILE651	-3.0	-2.3	ILE651	-4.3	-4.5
3.33	GLY652	-0.1	-0.1	GLY652	-0.2	-0.2	GLY652	-1.0	-1.0
3.35	SER654	-3.4	-3.4	SER654	-2.7	-2.1	SER654	-4.2	-3.6
3.36	PRO655	-5.3	-6.1	PRO655	-5.6	-5.9	PRO655	-4.7	-4.4
3.39	SER658	-1.4	-1.4	SER658	-2.2	-1.5	SER658	-1.9	-1.5
3.40	TYR659	-0.7	-0.7	TYR659	-1.3	-1.6	TYR659	-7.2	-5.3
5.40	VAL740	-0.7	-0.7	VAL740	-0.1	-0.1	VAL740	-0.5	-0.5
5.41	VAL741	-0.4	-0.5	VAL741	0.0	-0.0	VAL741	0.0	0.0
5.43	PRO743	0.0	0.0	PRO743	-0.2	-0.1	PRO743	-0.6	-1.0
5.44	LEU744	-0.8	-1.0	LEU744	-1.6	-1.6	LEU744	-2.4	-3.2
5.47	ASN747	-0.3	-0.1	ASN747	-0.5	-0.2	ASN747	-0.6	-0.7
5.51	ILE751	-0.1	-0.1	ILE751	-0.2	-0.1	ILE751	-1.2	-1.2
6.44	THR781	0.0	0.0	THR781	-0.3	-0.7	THR781	-1.4	-1.0
6.47	ILE784	-1.2	-0.6	ILE784	-0.7	-0.7	ILE784	-1.5	-1.5
6.48	TRP785	-0.9	-0.4	TRP785	-1.6	-1.4	TRP785	-2.2	-2.4
6.51	PHE788	-2.0	-2.1	PHE788	-3.1	-3.4	PHE788	-3.6	-4.0
6.55	TYR792	0.0	-0.9	TYR792	-0.1	0.0	TYR792	-0.7	-0.5
7.39	MET802	-0.4	-0.6	MET802	-0.9	-0.9	MET802	-1.7	-1.6
7.42	SER805	-5.5	-4.2	SER805	-3.2	-3.0	SER805	-2.4	-1.4
7.43	VAL806	-4.6	-4.6	VAL806	-4.0	-3.5	VAL806	-3.8	-4.1
7.44	SER807	-0.5	-0.4	SER807	-0.3	-0.1	SER807	-0.3	-0.2
7.45	LEU808	-0.6	-0.4	LEU808	-0.4	-0.2	LEU808	-0.2	-0.1
7.46	SER809	-4.6	-4.8	SER809	-7.3	-6.4	SER809	-3.2	-2.9
7.47	ALA810	-2.5	-2.7	ALA810	-1.9	-1.9	ALA810	-1.3	-1.2
7.50	ALA813	-0.6	-0.7	ALA813	-0.6	-0.9	ALA813	-1.1	-0.7

Persistent interactions are Identified

Four distinct protein-ligand interactions are observed: hydrogen bonds, hydrophobic contact, ionic interaction, and water bridges. Hydrogen bonds are broken down into four subtypes: backbone acceptor, backbone donor, side-chain acceptor, and side-chain donor. Hydrophobic interactions include π -Cation interaction between hydrophobic acids acid to an

aromatic or aliphatic group on the ligand. The ionic interactions or polar interactions are simply interactions between two oppositely charged atoms and do not involve a hydrogen bond. The water bridges are hydrogen bonds formed between water molecules that are geometrically relaxed. A protein-ligand interaction 2D diagram and histogram for each system averaged over the three individual trajectories are available in Figure 4 and those for the three individual trajectories are in Figures S9-S11.

Our simulations reveal key interactions between mGluR5 and the ligands. These interactions contribute much to the strong binding formed by the PAM CDPPB. This ligand forms more interactions—mostly hydrophobic, and hydrogen bonds with Ser654^{3.39} and Ser809^{7.46} (the superscript denotes Ballesteros-Weinstein numbering) [41], of which Ser654^{3.39} is found to be unique to the PAM CDPPB system (**Figure 4**).

The local changes of the NAMs, and PAM-CDPPB bound mGluR5 are shown based on the protein C-α root-mean-square fluctuation (RMSF) (Figure 5). The highest peak indicates the area where the protein fluctuates the most during the simulation. N- and C-terminal regions as well as the intracellular and extracellular loop usually experience the highest fluctuation [42]. For the three individual trajectories, the protein RMSF of each system is available in Figures S12-S15. The calculated average ligand RMSF values are 0.60 Å, 0.95 Å, and 0.99 Å, for MFZ10-7, MTEP and CDPPB, respectively. For each system, the ligand RMSF for the three individual trajectories can be found in Figures S16-S18. Structurally, both NAMs exhibit rigidity because of the triple bond. The PAM, CDPPB, on the other hand, is more molecularly flexible, as it contains five rotatable bonds. Figure S19 illustrates the ligand torsion plot for the CDPPB.

Secondary structures (alpha helices and beta strands) are computed over the three trajectories for each system. Alpha helical content is found to be approximately 64.15% for the

receptor with MTEP, 62.60% for the receptor with MFZ10-7, and 63.68% for the receptor with CDPPB (Figure 6). Overall, the three systems show subtle differences at helices TM3 and TM5. At both TMs, there appears to be a little bit more helical content for the receptor bound by the PAM CDPPB than that bound by the NAM ligands. The illustration of the protein secondary distribution for the three corresponding MD simulation trajectories can be found in Figures S20-S22. The beta-strand content remains at 0.00% for all three systems, while the alpha-helical distributions do not vary significantly between the NAMs and the PAM.

The PAM CDPPB induces larger conformational changes

The NAM systems show relatively smaller conformational changes at the TMD (**Figures 3A and B**). On the other hand, the PAM CDPPB system displays the larger conformational change at TM4, TM5 and TM7 (**Figure 3C**). While TM4 appears to shift inward in the PAM CDPPB system, the same helix does not change much in the NAM MFZ10-7 system, and in the crystal structure of mGluR5 (4009) [24].

Molecular switches in mGluR5

Molecular switches are a set of, usually, conserved structural motifs that are involved in signal transduction in GPCRs. These switches include the tyrosine toggle switch, transmission switch, and ionic lock switch. **Figure 7** shows molecular switch analysis between the NAM MFZ10-7 and PAM CDPPB bound system. The ionic lock, which is a salt bridge between K665^{3.50} and E770^{6.35}, appears to be broken in the PAM CDPPB bound mGluR5. The distances between K665^{3.50} and E770^{6.35} are 3.8 Å and 6.6 Å for MFZ10-7 and CDPPB, respectively (**Table 3**). The transmission switch at TM6, C1XW does not show a significant change between the two systems. Also, the conserved toggle switch residues H/Y/HxPKxY in mGluR5 appear to

perform the same role as the NPxxY(x)F motif in class A GPCRs [24], does not show a significant difference between the two systems.

Table 3. Conserved molecular switches within mGluR5 and their respective distances between residues involved.

MFZ10-7/CDPPB	Residues	Distance (Å)
Toggle	Tyr823 ¹ :OH– Tyr832 ² :OH	1.8
Transmission	Glu770 ¹ -Glu770 ²	2.5
Ionic lock (NAM MFZ10-7)	Lys665 ¹ -Glu770 ¹	3.8
Ionic lock (PAM CDPPB)	Lys665 ² -Glu770 ²	6.6

¹mGluR5-MFZ10-7 complex structure

Discussion

To date, no crystal structures of mGluR5 complexed with PAM have been reported despite the therapeutic potential of the PAM in the treatment of schizophrenia and cognitive disorders[15]. In this study, molecular docking reveals that the PAM CDPPB binds to mGluR5 with higher affinity and occupies greater volume of the mGluR5 allosteric modulation site compared with NAMs. Consistent with the docking scores, the estimated MM/GBSA binding energy of the PAM CDPPB is higher than those of the NAMs. The MM/GBSA binding energy score is considered more reliable for predicting ligand-binding affinities with improved accuracy [43]. The stronger binding of the PAM to the receptor is achieved by the formation of unique persistent interactions with SER654^{3,35} via NH group deep in the pocket.

The PAM-bound system demonstrates subtle conformational change at TM3 and TM7 (Figure S23). The motion of TM7 is likely to be felt by the C-terminal intracellular region, whose conformational change determines the activation state of several GPCRs [42, 44]. To

²mGluR5-CDPPB complex structure

compare our simulated systems with the experimental data, the most abundant structures of the NAMs, and PAM CDPPB bound mGluR5 derived from the MD simulations were superimposed with the crystal structures of mGluR5 complexed with the NAM mavoglurant (4009) [24], apo form (PDB ID: 6N52) [20], agonist (PDB ID: 6N51) [20], and antagonist-bound mGluR5 (PDB ID: 3FD9) [45] (Figures 8-10). The NAM-bound systems are found to have smaller RMSD values with respect to the NAM-bound crystal structure, the apo form, and to some extent, the antagonist-bound crystal structure, but show significant structural differences when compared to the agonist-bound crystal structure. On the other hand, the PAM CDPPB-bound system is found to have a reduced RMSD when superimposed with the agonist-bound crystal structure (**Table 4**). Thus, the simulations may have predicted the PAM CDPPB-bound mGluR5 to be closer to the agonist-bound crystal structure [20] than the apo [20], the NAM [24], and the antagonist-bound crystal structures [45]. However, the differences between the calculated RMSDs may be insignificant and inconclusive given that they were based on a single experimental structure. Also, the fact that we used only one PAM ligand to characterize the conformational changes, we may not capture accurately those differences. Nonetheless, these data may suggest that PAM works by inducing conformational changes to the receptor.

Table 4. Structural alignment of mGluR5 MD simulation systems with apo, NAM, agonist, and antagonist bound crystal structures. MD: the most abundant conformation from the MD simulations.

	RMSD (Å)							
	NAM mavoglurant (4009)	NAM NFZ10-7 (MD)	NAM MTEP (MD)	PAM CDPPB (MD)	Apo (6N52)	Antagonist (7FD9)	Agonist (6N51)	
NAM (4009)		2.94	3.00	3.48	3.09	3.59	4.20	
NAM MFZ10-7 (MD)			2.40	3.98	3.89	4.11	4.42	
NAM MTEP (MD)				3.17	3.85	4.02	4.46	
PAM CDPPB (MD)					3.94	4.17	3.69	
Apo (6N52)								
Agonist (6N51)						5.87		
Antagonist (6N51)								

Furthermore, potential molecular switches in GPCRs were examined. These include a set of non-covalent interactions whose disturbances allow a receptor to enter an activated state [46] while those sequences similar to the toggle switch and transmission switch in class A GPCRs [24], do not change over time, a salt bridge between TM3 and TM7, which corresponds to the ionic lock the class A GPCRs is broken in the PAM system. This salt bridge breakage may be related to the larger conformational changes observed at these helices upon binding of the PAM CDPPB. This agrees with a report that a potential activation switch holds TM7, TM3 and TM6 together at the base of the pocket [21].

A previous MD study used enhanced molecular dynamics simulations to analyze the actions of a PAM ligand (3,3'-difluorobenzaldazine/DFB) with reference to a NAM ligand (m-MPEP) on TMD of mGluR5 [47]. The study analyzed the probability of the depth of the ligands inside the pocket sampled in the three systems that are measured by the center-of-mass distance between the ligand and the $C\alpha$ atoms of the triad residues including Tyr659^{3.44}, Thr781^{6.46}, Ser809^{7.39} [47]. In MD simulations, the dual binding mode of the PAM was observed in wt-DFB

while wt-m-MPEP but mut-DFB exhibited only one binding mode for the NAMs [47].

Additionally, it was suggested that intrinsic efficacy of mGluR5 can be associated with a shift to a shallower pocket that causes rotation of Phe788^{6.53} and displacement of TM6 relatively to TM7 altering triad confirmation [47]. These findings suggest that PAM induces conformational changes in TMD, resembling class A GPCR activation of mGluR5 and dual binding modes with a shallower one contributing to its allosteric agonism [47]. In our study, similar analysis has been performed to calculate probability distribution of the depth of the NAM ligands and PAM CDPPB based on the same residues of mGluR5. Consistently, our findings demonstrate a distance of approximately 5.5 Å for both NAMs and an increased distance of 6.5 Å for PAM, indicating a shift to a shallower pocket (Figure S24). In contrast, however, only one binding pocket for PAM CDPPB is observed in our study. Therefore, this study may aid in the design of PAMs with improved binding properties to the mGluR5 for possible treatment of schizophrenia and cognitive disorders.

Conclusions

Despite the therapeutic potential of the mGluR5 PAM no crystal structure of the receptor complexed with PAM is available, hence the structural basis of the ligand binding is poorly understood. We studied the binding of PAM CDPPB to the mGluR5 using microsecond MD simulations. Our data suggest conformational changes of the PAM CDPPB-bound mGluR5. The PAM-induced receptor conformation is more like the agonist induced conformation than the antagonist-induced conformation, suggesting that PAM works by stabilizing the active conformation. These findings may aid the design of better mGluR5 PAMs for the treatment of schizophrenia and cognitive disorders.

Acknowledgments

C.W acknowledges the support by the New Jersey Health Foundation (PC 76-21) and the National Science Foundation under Grants NSF ACI-1429467/RUI-1904797, and XSEDE MCB 170088. The Anton2 machine at the Pittsburgh Supercomputing Center (MCB170090P) was generously made available by D. E. Shaw Research.

References

- 1. Pellicciari, R. and G. Costantino, *Metabotropic G-protein-coupled glutamate receptors as therapeutic targets*. Current Opinion in Chemical Biology, 1999. **3**(4): p. 433-440.
- 2. Caraci, F., et al., *Metabotropic glutamate receptors in neurodegeneration/neuroprotection: Still a hot topic?* Neurochemistry International, 2012. **61**(4): p. 559-565.
- 3. Walker, K., et al., Metabotropic glutamate receptor subtype 5 (mGlu5) and nociceptive function I. Selective blockade of mGlu5 receptors in models of acute, persistent and chronic pain.

 Neuropharmacology, 2001. **40**(1): p. 1-9.
- 4. Guimaraes, I.M., et al., *The metabotropic glutamate receptor 5 role on motor behavior involves specific neural substrates.* Molecular Brain, 2015. **8**(1).
- 5. Reiner, A. and J. Levitz, *Glutamatergic Signaling in the Central Nervous System: Ionotropic and Metabotropic Receptors in Concert.* Neuron, 2018. **98**(6): p. 1080-1098.
- 6. Brown, R.M., et al., *mGlu5 Receptor Functional Interactions and Addiction*. Frontiers in Pharmacology, 2012. **3**.
- 7. Tan, S.Z.K. and J.H. Kim, *mGlu5: A double-edged sword for aversive learning related therapeutics.* Neuroanatomy and Behaviour, 2021. **3**.
- 8. Niswender, C.M. and P.J. Conn, *Metabotropic Glutamate Receptors: Physiology, Pharmacology, and Disease.* Annual Review of Pharmacology and Toxicology, 2010. **50**(1): p. 295-322.
- 9. Nickols, H.H. and P.J. Conn, *Development of allosteric modulators of GPCRs for treatment of CNS disorders*. Neurobiology of Disease, 2014. **61**: p. 55-71.
- 10. Smith, N.J., G. Milligan, and D. Sibley, *Allostery at G Protein-Coupled Receptor Homo- and Heteromers: Uncharted Pharmacological Landscapes.* Pharmacological Reviews, 2010. **62**(4): p. 701-725.
- 11. Emmitte, K.A., *mGlu5 negative allosteric modulators: a patent review (2013 2016).* Expert Opin Ther Pat, 2017. **27**(6): p. 691-706.
- 12. Zeidler, S., et al., *Combination Therapy in Fragile X Syndrome; Possibilities and Pitfalls Illustrated by Targeting the mGluR5 and GABA Pathway Simultaneously.* Frontiers in Molecular Neuroscience, 2017. **10**.
- 13. Silverman, J.L., et al., Negative Allosteric Modulation of the mGluR5 Receptor Reduces Repetitive Behaviors and Rescues Social Deficits in Mouse Models of Autism. Science Translational Medicine, 2012. **4**(131).
- 14. Keck, T.M., et al., *A novel mGluR5 antagonist, MFZ 10-7, inhibits cocaine-taking and cocaine-seeking behavior in rats.* Addiction Biology, 2014. **19**(2): p. 195-209.

- 15. Lecourtier, L., et al., *Positive Allosteric Modulation of Metabotropic Glutamate 5 (mGlu5)*Receptors Reverses N-Methyl-D-Aspartate Antagonist-Induced Alteration of Neuronal Firing in Prefrontal Cortex. Biological Psychiatry, 2007. **62**(7): p. 739-746.
- 16. Olive, M.F., Cognitive effects of Group I metabotropic glutamate receptor ligands in the context of drug addiction. European Journal of Pharmacology, 2010. **639**(1-3): p. 47-58.
- 17. Nicoletti, F., et al., *Targeting mGlu Receptors for Optimization of Antipsychotic Activity and Disease-Modifying Effect in Schizophrenia*. Frontiers in Psychiatry, 2019. **10**.
- 18. Kinney, G.G., et al., A Novel Selective Positive Allosteric Modulator of Metabotropic Glutamate Receptor Subtype 5 Has in Vivo Activity and Antipsychotic-Like Effects in Rat Behavioral Models. Journal of Pharmacology and Experimental Therapeutics, 2005. **313**(1): p. 199-206.
- 19. Stauffer, S.R., *Progress toward positive allosteric modulators of the metabotropic glutamate receptor subtype 5 (mGluR5)*. ACS Chem Neurosci, 2011. **2**(8): p. 450-70.
- 20. Koehl, A., et al., *Structural insights into the activation of metabotropic glutamate receptors.* Nature, 2019. **566**(7742): p. 79-84.
- 21. Dore, A.S., et al., *Structure of class C GPCR metabotropic glutamate receptor 5 transmembrane domain.* Nature, 2014. **511**(7511): p. 557-62.
- 22. Christopher, J.A., et al., Fragment and Structure-Based Drug Discovery for a Class C GPCR: Discovery of the mGlu5 Negative Allosteric Modulator HTL14242 (3-Chloro-5-[6-(5-fluoropyridin-2-yl)pyrimidin-4-yl]benzonitrile). J Med Chem, 2015. **58**(16): p. 6653-64.
- 23. Nasrallah, C., et al., *Agonists and allosteric modulators promote signaling from different metabotropic glutamate receptor 5 conformations.* Cell Rep, 2021. **36**(9): p. 109648.
- 24. Doré, A.S., et al., *Structure of class C GPCR metabotropic glutamate receptor 5 transmembrane domain.* Nature, 2014. **511**(7511): p. 557-562.
- 25. Sastry, G.M., et al., *Protein and ligand preparation: parameters, protocols, and influence on virtual screening enrichments.* J Comput Aided Mol Des, 2013. **27**(3): p. 221-34.
- 26. Harder, E., et al., *OPLS3: A Force Field Providing Broad Coverage of Drug-like Small Molecules and Proteins.* J Chem Theory Comput, 2016. **12**(1): p. 281-96.
- 27. Friesner, R.A., et al., *Glide: a new approach for rapid, accurate docking and scoring. 1. Method and assessment of docking accuracy.* J Med Chem, 2004. **47**(7): p. 1739-49.
- 28. Lomize, M.A., et al., *OPM database and PPM web server: resources for positioning of proteins in membranes.* Nucleic Acids Research, 2012. **40**(D1): p. D370-D376.
- 29. Lyman, E., et al., A role for a specific cholesterol interaction in stabilizing the Apo configuration of the human A(2A) adenosine receptor. Structure, 2009. **17**(12): p. 1660-1668.
- 30. Uba, A.I., et al., *Elucidation of partial activation of cannabinoid receptor type 2 and identification of potential partial agonists: Molecular dynamics simulation and structure-based virtual screening.* Computational Biology and Chemistry, 2022. **99**.
- 31. Uba, A.I., et al., Activation Mechanism of Corticotrophin Releasing Factor Receptor Type 1 Elucidated Using Molecular Dynamics Simulations. ACS Chemical Neuroscience, 2021. **12**(9): p. 1674-1687.
- 32. Kevin J. Bowers, E.C., Huafeng Xu, Ron O. Dror, Michael P. Eastwood,, J.L.K. Brent A. Gregersen, Istvan Kolossvary, Mark A. Moraes, Federico D. Sacerdoti,, and Y.S. John K. Salmon, David E. Shaw, Scalable Algorithms for Molecular Dynamics Simulations on Commodity Clusters. 2006.
- 33. Ikeguchi, M., *Partial Rigid-Body Dynamics in NPT, NPAT and NPgammaT Ensembles for Proteins and Membranes.* J. Comput. Chem., 2004. **25**(4): p. 529-541.
- 34. Bailey, A.G. and C.P. Lowe, *MILCH SHAKE: An Efficient Method for Constraint Dynamics Applied to Alkanes.* J. Comput. Chem., 2009. **30**(15): p. 2485-2493.

- 35. Shan, Y., et al., *Gaussian Split Ewald: A Fast Ewald Mesh Method for Molecular Simulation.* J. Chem. Phys., 2005. **122**(5): p. 54101-54101.
- 36. Stuart, S.J., R. Zhou, and B.J. Berne, *Molecular Dynamics with Multiple Time Scales: The Selection of Efficient Reference System Propagators.* J. Chem. Phys., 1996. **105**(4): p. 1426-1436.
- 37. Bowers, K.J., et al., *Scalable algorithms for molecular dynamics simulations on commodity clusters*, in *Proceedings of the 2006 ACM/IEEE conference on Supercomputing*. 2006, ACM: Tampa, Florida. p. 84.
- 38. Wang, C., et al., *Recent Developments and Applications of the MMPBSA Method.* Front Mol Biosci, 2017. **4**: p. 87.
- 39. Li, J., et al., *The VSGB 2.0 model: A next generation energy model for high resolution protein structure modeling.* Proteins: Structure, Function, and Bioinformatics, 2011. **79**(10): p. 2794-2812.
- 40. Ghosh, A., C.S. Rapp, and R.A. Friesner, *Generalized Born Model Based on a Surface Integral Formulation.* J. Phys. Chem. B, 1998. **102**(52): p. 10983-10990.
- 41. Ballesteros, J.A. and H. Weinstein, [19] Integrated methods for the construction of three-dimensional models and computational probing of structure-function relations in G protein-coupled receptors, in Receptor Molecular Biology. 1995. p. 366-428.
- 42. Uba, A.I., et al., *Binding of agonist WAY-267,464 and antagonist WAY-methylated to oxytocin receptor probed by all-atom molecular dynamics simulations.* Life Sciences, 2020. **252**.
- 43. Kollman, P.A., et al., *Calculating Structures and Free Energies of Complex Molecules: Combining Molecular Mechanics and Continuum Models.* Accounts of Chemical Research, 2000. **33**(12): p. 889-897.
- 44. Sato, T., et al., Functional Role of the C-Terminal Amphipathic Helix 8 of Olfactory Receptors and Other G Protein-Coupled Receptors. International Journal of Molecular Sciences, 2016. **17**(11).
- 45. Nasrallah, C., et al., *Agonists and allosteric modulators promote signaling from different metabotropic glutamate receptor 5 conformations.* Cell Reports, 2021. **36**(9).
- 46. Filipek, S., *Molecular switches in GPCRs*. Current Opinion in Structural Biology, 2019. **55**: p. 114-120.
- 47. Cong, X.J., et al., *Allosteric Modulation Mechanism of the mGluR(5) Transmembrane Domain.*Journal of Chemical Information and Modeling, 2019. **59**(6): p. 2871-2878.

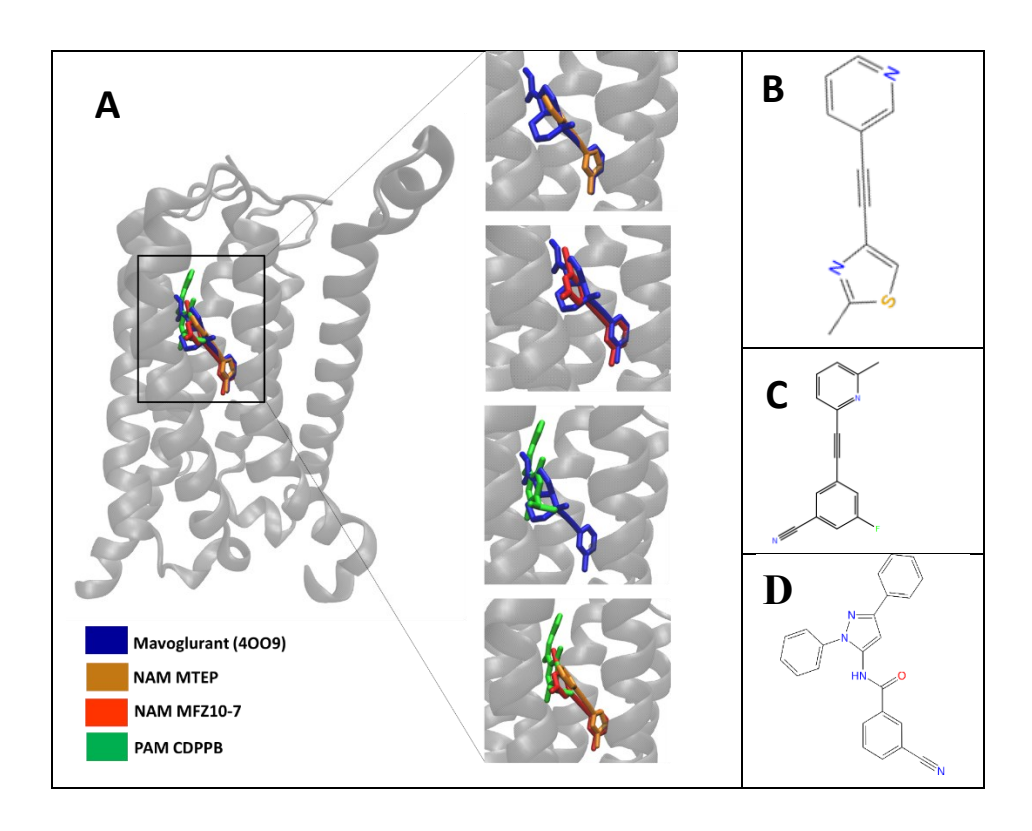


Figure 1. Superimposition of the docking poses of NAMs MTEP, MFZ 10-7, and PAM CDPPB with the cocrystal pose of mavoglurant (PDB id 4OO9). The NAMs and PAM were docked into the allosteric site of mGlu5R. B: MTEP, C: MFZ 10-7, and D: CDPPB.

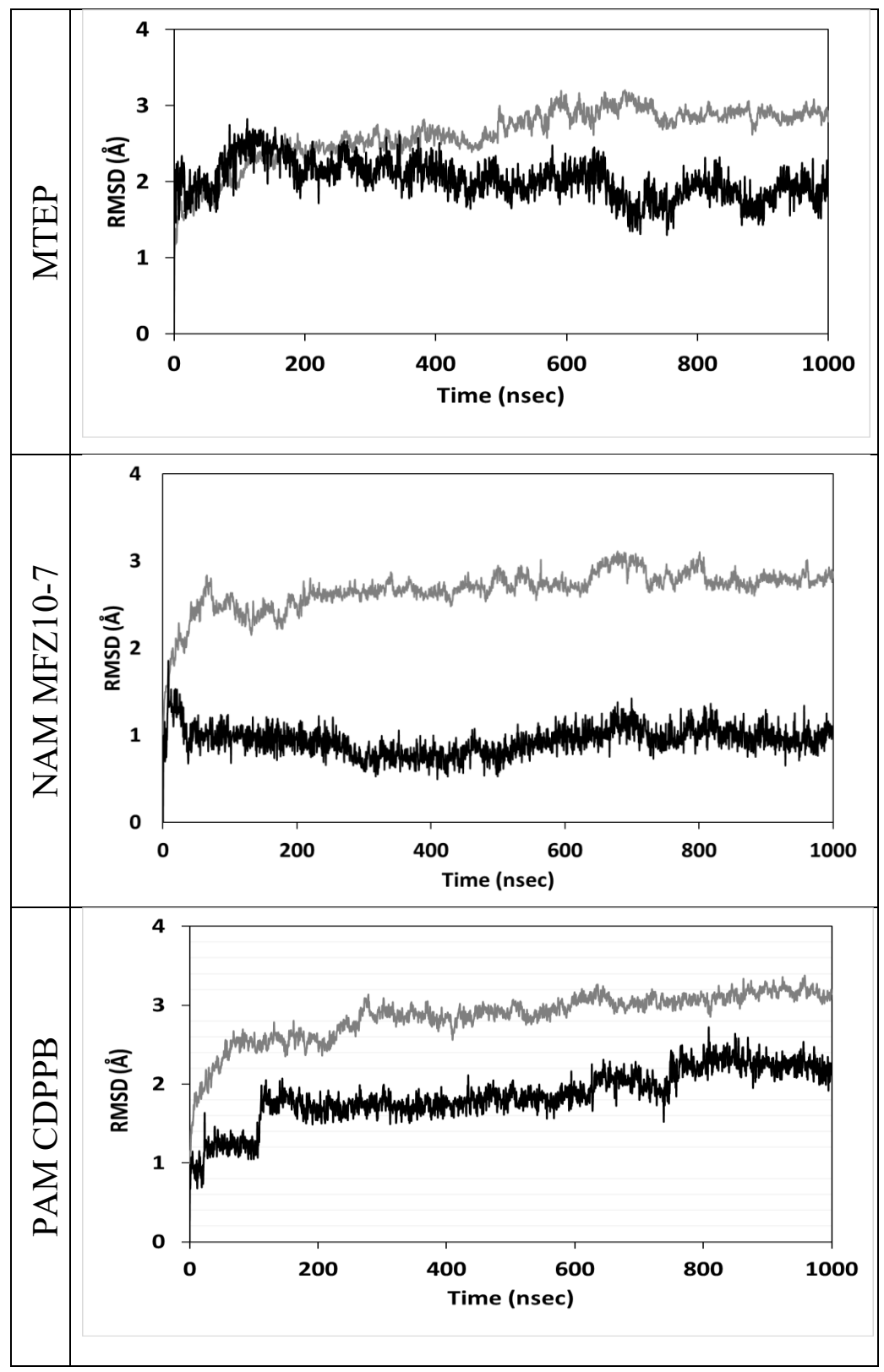


Figure 2. Root Mean Square Deviation (RMSD) of protein-Ligand complexes averaged over three trajectories for each system. Cα-RMSD in grey is measured using the initial frame as a reference, while the ligand fit on protein RMSD refers to in place RMSD of ligand in black when protein is aligned.

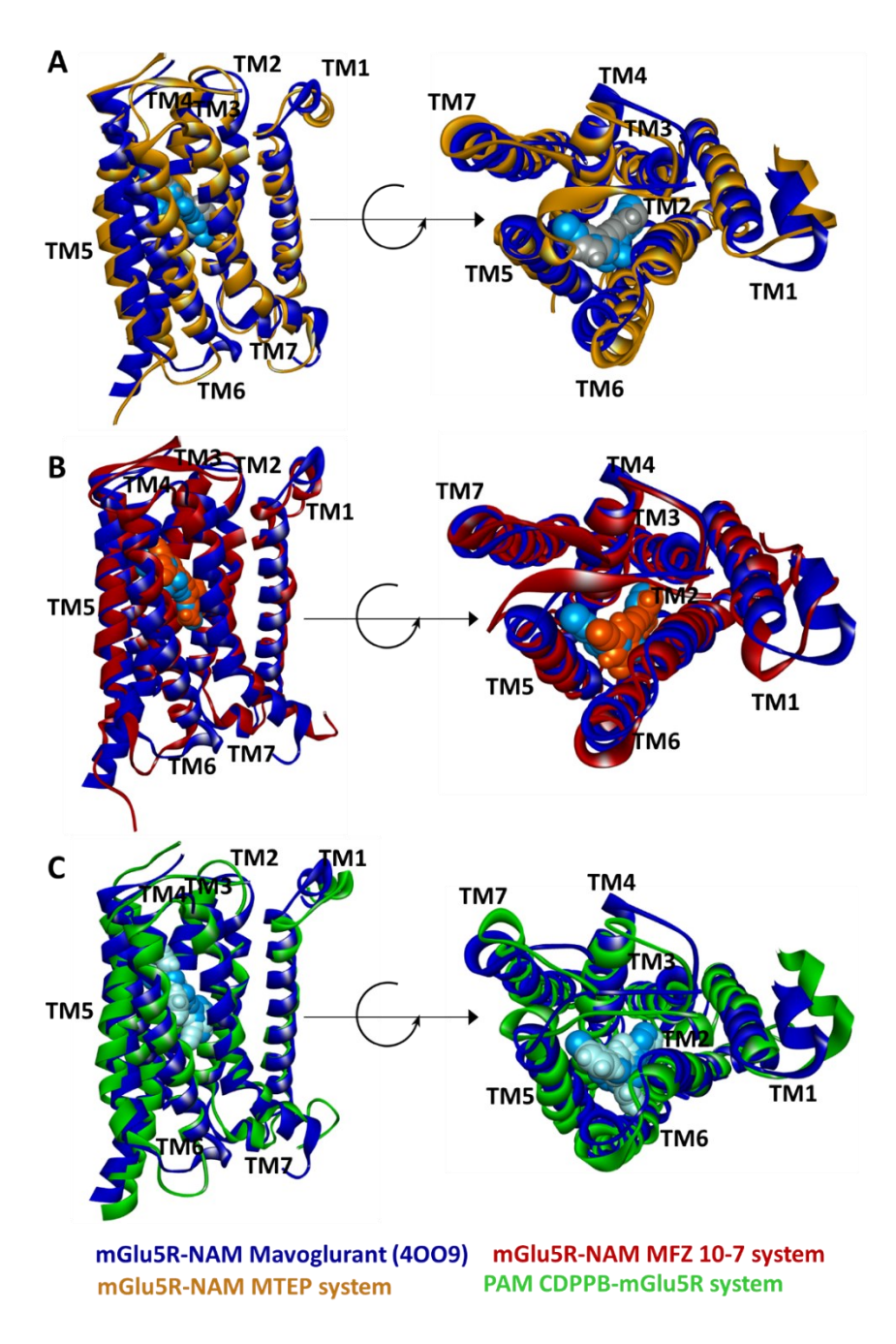


Figure 3. Superimposition of the cocrystal pose of mavoglurant in the crystal structure of NAM mavoglurant bound mGluR5 (PDB ID: 4OO9) with the most abundant structures obtained from MD simulation of (A) NAM MTEP, (B) NAM MFZ 10-7, (C) PAM CDPPB.

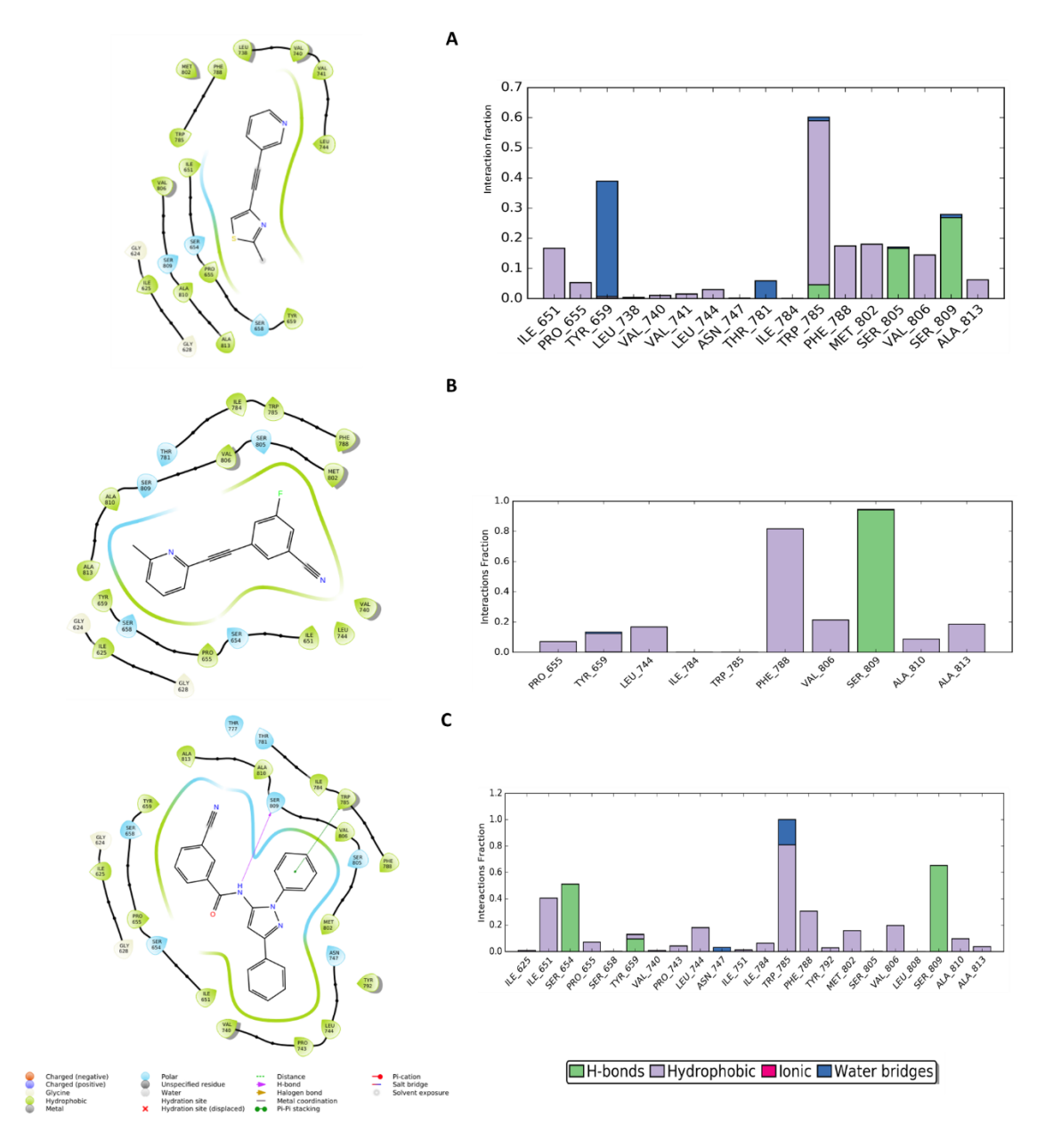


Figure 4. Protein-ligand interaction for the most abundant structure (left) and histogram showing interaction fraction over time (right): (A) MTEP, (B)MFZ10-7, and (C) CPPDB.

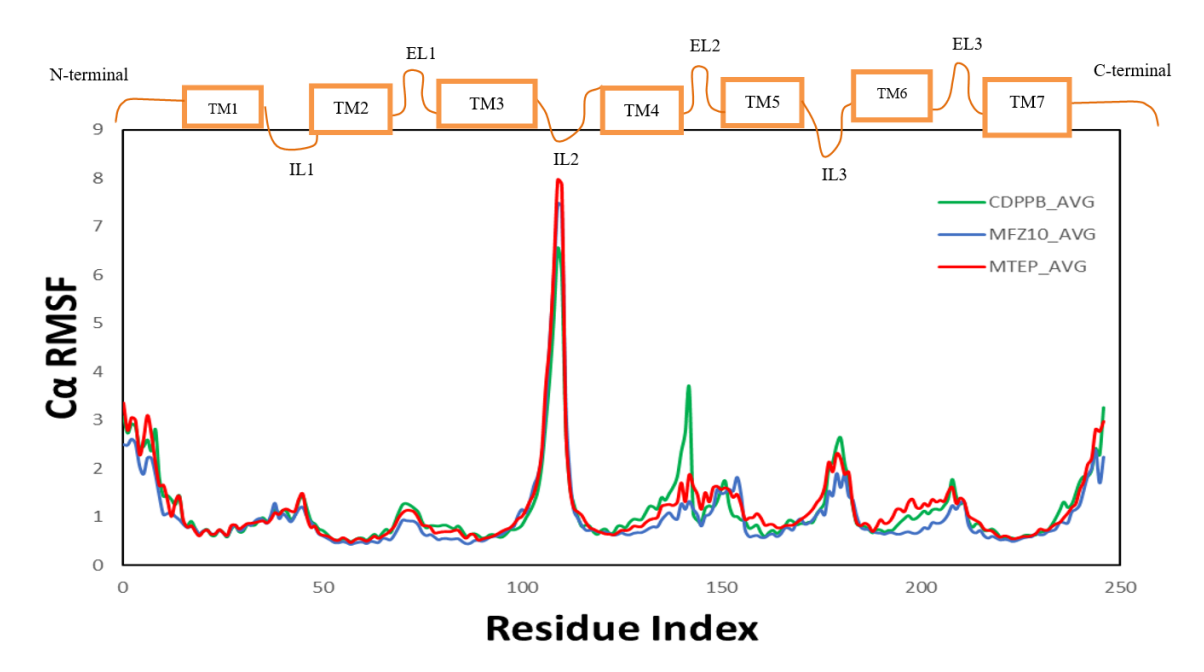


Figure 5. C α RMSF (Root mean-square-fluctuation) comparison of two NAMs, and PAM CDPPB bound to the receptor mGluR5 averaged over the three trajectories for each ligand system. The C α RMSF value is a measure of how much the protein changes conformation at a specific residue. TM denotes transmembrane domains 1-7; IL: intercellular loops 1-3; EL: extracellular loops 1-3.

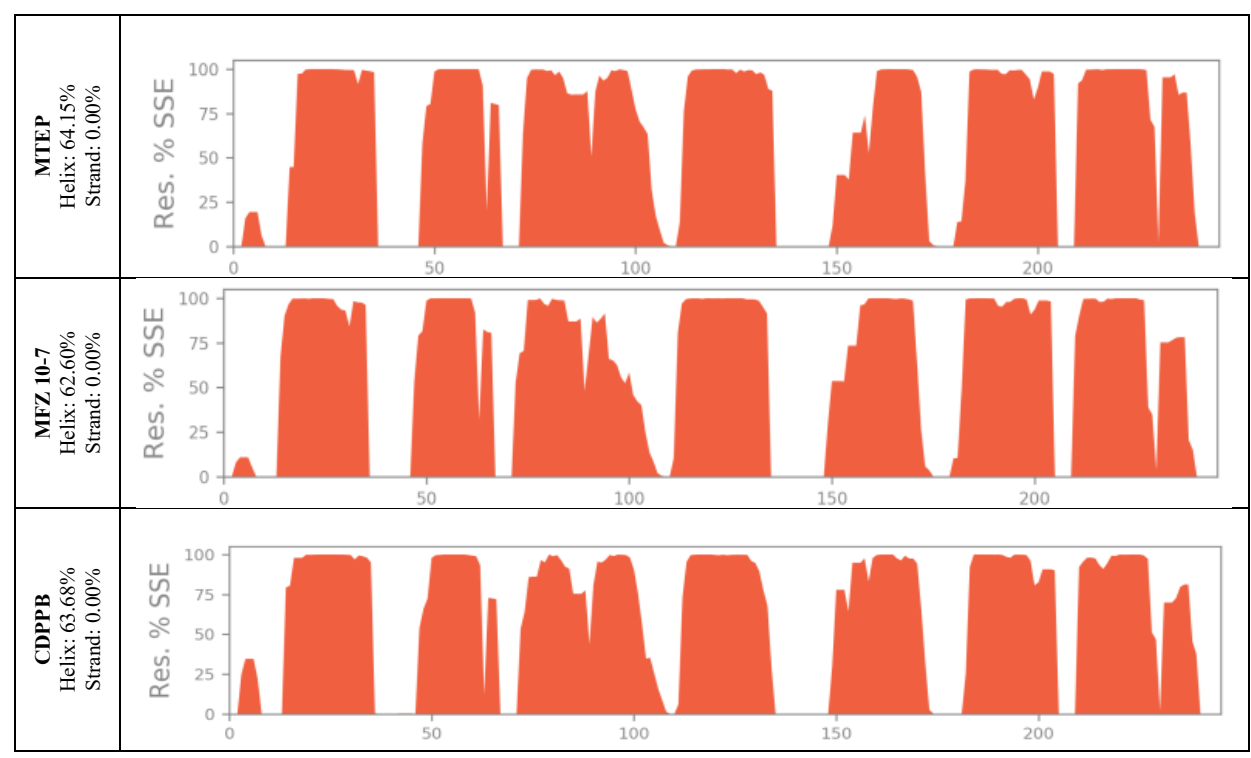


Figure 6. Illustration of the protein secondary distribution for MTEP, MFZ 10-7, and CDPPB averaged over the three MD trajectories. Alpha helix (bed), beta strand (blue). The beta strand content is 0.00%.

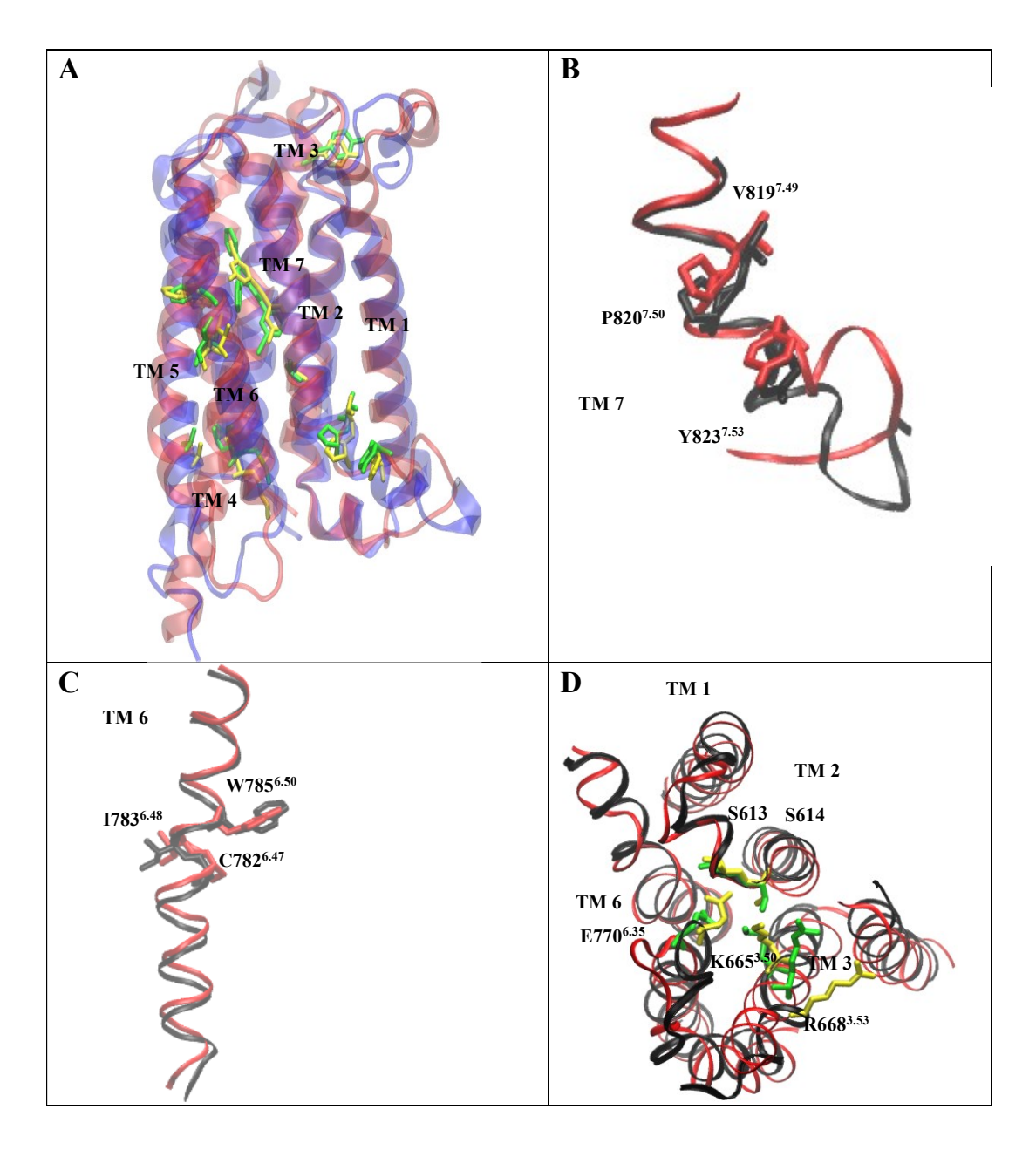


Figure 7. **A** MFZ 10-7 and CDPPB ligands in complex with mGluR5 (MFZ 10-7/mGluR5: blue/yellow; CDPPB/mGluR5: red/green). **B**. Tyrosine Toggle Switch **C**. Transmission Switch **D**. Ionic Lock Switch. **B-D**. MFZ 10-7/mGluR5: black; CDPPB/mGluR5: red.

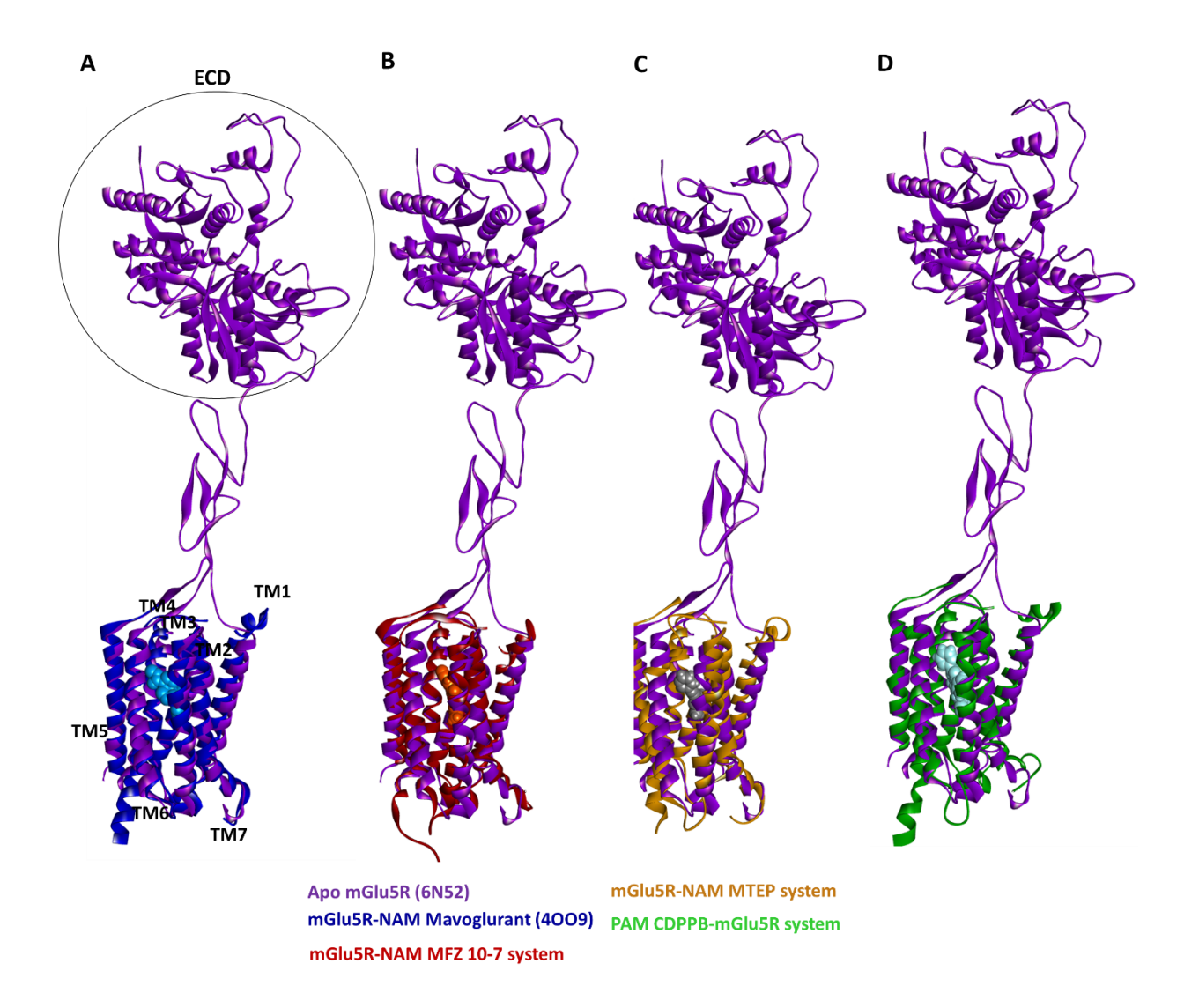


Figure 8. Superimposition of the crystal structure of NAM mavoglurant bound mGluR5 (4009) and MD simulation complexes of NAM and PAM bound mGluR5 with the full-length apo form: (A) crystal structure of mGluR5 complexed with NAM mavoglurant, (B) NAM MFZ 10-7 bound mGluR5, (C) NAM MTEP bound mGluR5, (D) PAM CDPPB bound mGluR5. ECD denotes the N-terminal extracellular domain, TM denotes transmembrane helices (1-7).

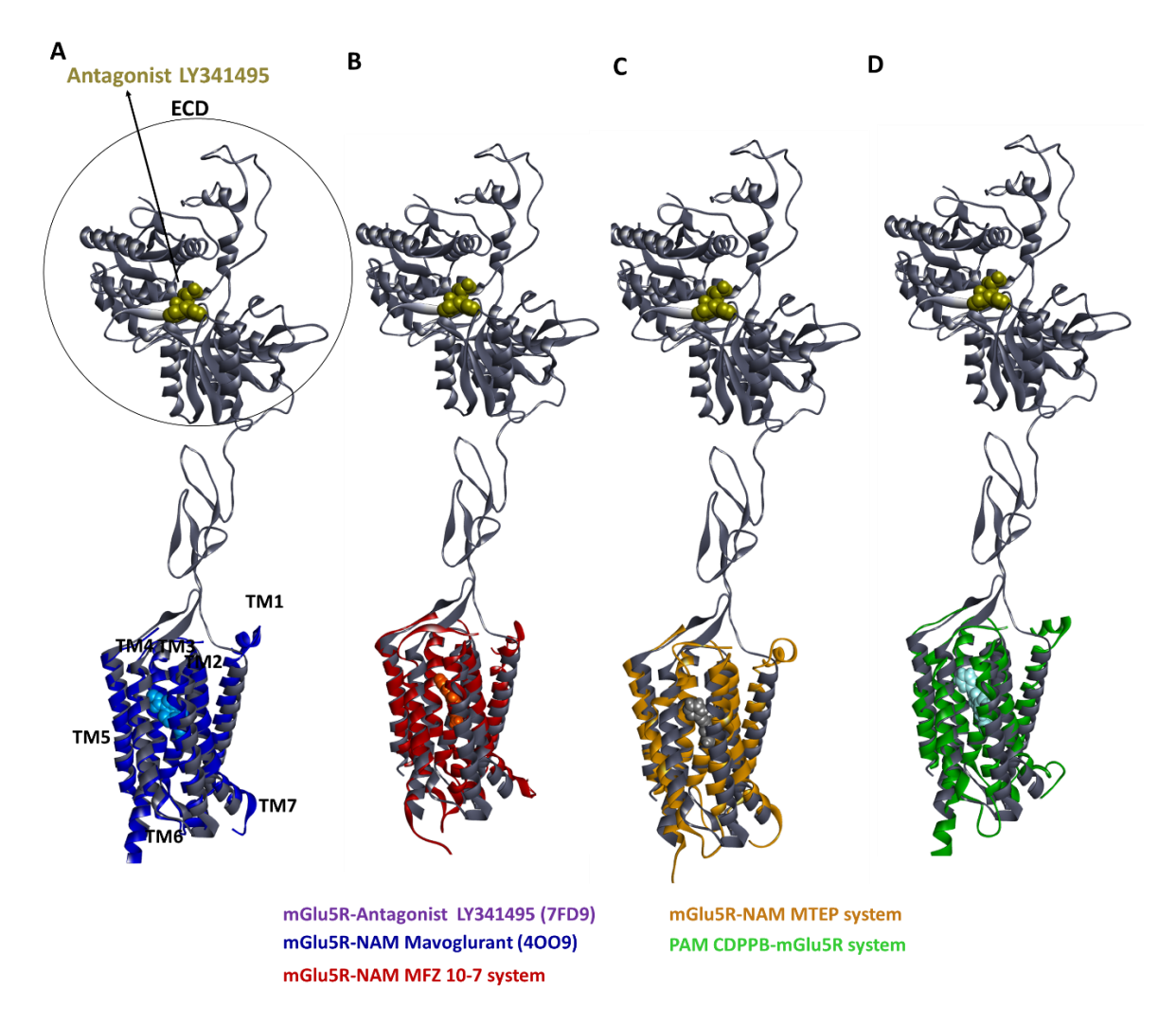


Figure 9. Superimposition of the crystal structure of NAM mavoglurant bound mGluR5 (PDB id: 4OO9) and MD simulation complexes of NAM and PAM bound mGluR5 with the full-length antagonist bound mGluR5 (PDB id: 7FD9): (A) crystal structure of mGluR5 complexed with NAM mavoglurant, (B) NAM MFZ 10-7 bound mGluR5, (C) NAM MTEP bound mGluR5, (D) PAM CDPPB bound mGluR5. ECD denotes the N-terminal extracellular domain, TM denotes transmembrane helices (1-7).

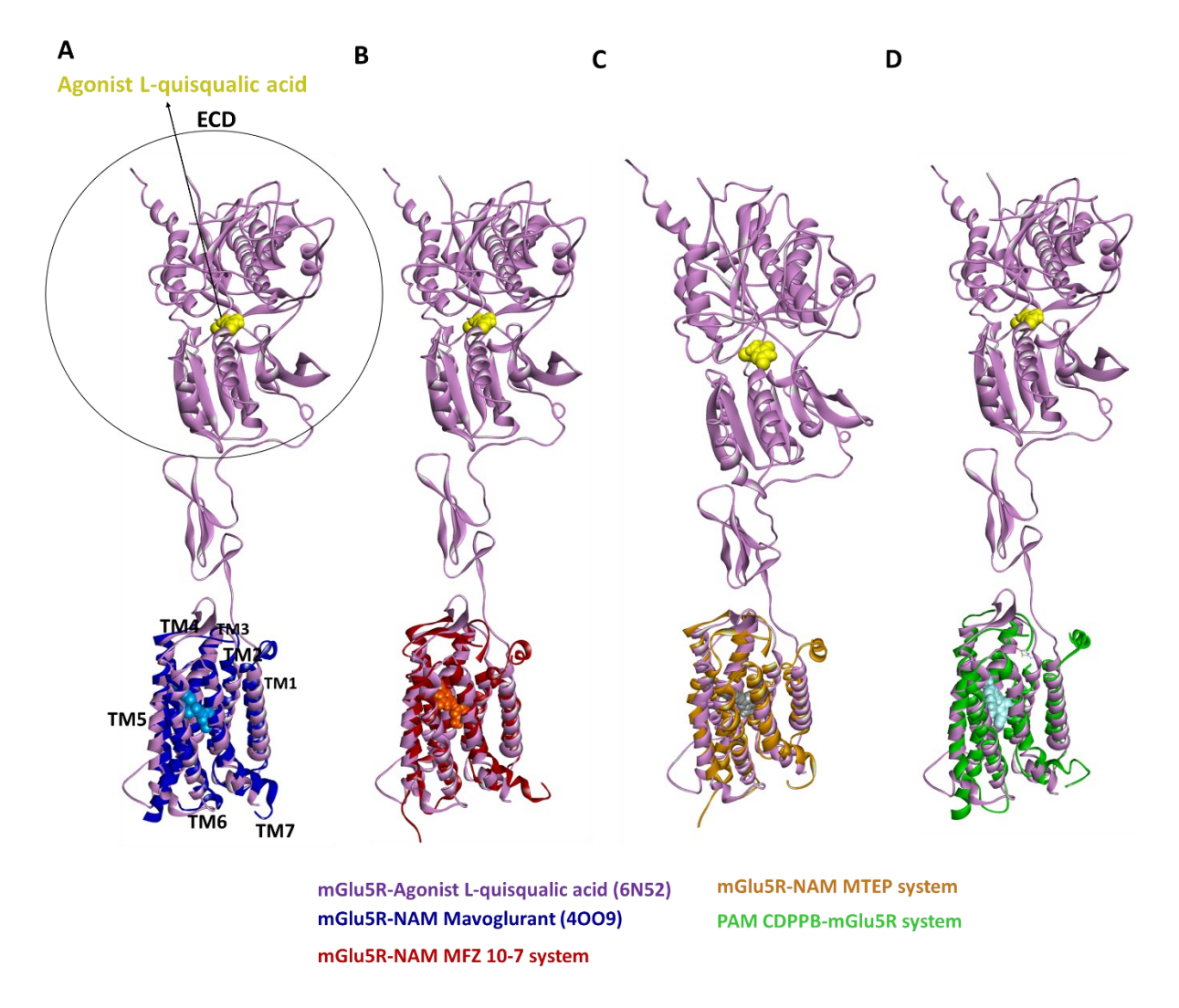


Figure 10. Superimposition of the crystal structure of NAM mavoglurant bound mGluR5 (PDB id: 4009) and MD simulation complexes of NAM and PAM bound mGluR5 with the full-length antagonist bound mGluR5 (PDB id: 7FD9): (A) crystal structure of mGluR5 complexed with NAM mavoglurant, (B) NAM MFZ 10-7 bound mGluR5, (C) NAM MTEP bound mGluR5, (D) PAM CDPPB bound mGluR5.